

RESEARCH

Open Access



Exosomal lncRNA Mir100hg from lung cancer stem cells activates H3K14 lactylation to enhance metastatic activity in non-stem lung cancer cells

Lei Shi^{1,4†}, Bowen Li^{1†}, Jiyu Tan^{1†}, Ling Zhu^{3†}, Sicheng Zhang¹, Yuhan Zhang¹, Meng Xiang¹, Jie Li², Yan Chen¹, Xue Han², Jiacheng Xie¹, Yao Tang¹, H. Rosie Xing^{1*}, Jingyu Li^{3*} and Jianyu Wang^{2*}

Abstract

The mean survival of metastatic lung adenocarcinoma is less than 1 year, highlighting the urgent need to understand the mechanisms underlying its high mortality rate. The role of Extracellular vesicles (EVs) in facilitating the interactions between cancer cells and the metastatic microenvironment has garnered increasing attention. Previous studies on the role of EVs in metastasis have been primarily focused on cancer cell-derived EVs in modulating the functions of stromal cells. However, whether cancer stem cells (CSCs) can alter the metastatic properties of non-CSC cells, and whether EV crosstalk can mediate such interaction, have not been demonstrated prior to this report. In the present study, we integrated multi-omics sequencing and public database analysis with experimental validation to demonstrate, for the first time, the exosomal Mir100hg, derived from CSCs, could enhance the metastatic potential of non-CSCs both in vitro and in vivo. Mechanistically, HNRNPF and HNRNPA2B1 directly binds to Mir100hg, facilitating its trafficking via exosomes to non-CSCs. In non-CSCs, Mir100hg upregulates ALDOA expression, subsequently leading to elevated lactate production. Consequently, the increased lactate levels enhance H3K14 lactylation by 2.5-fold and promote the transcription of 169 metastasis-related genes. This cascade of events ultimately results in enhanced ALDOA-driven glycolysis and histone lactylation-mediated metastatic potential of non-CSC lung cancer cells. We have delineated a complex regulatory network utilized by CSCs to transfer their high metastatic activity to non-CSCs through exosomal Mir100hg, providing new mechanistic insights into the communication between these two heterogeneous tumor cell populations. These mechanistic insights provide novel therapeutic targets for metastatic lung cancer, including HNRNPF/HNRNPA2B1-mediated Mir100hg trafficking and the histone lactylation pathway, advancing our understanding of CSC-mediated metastasis while suggesting promising strategies for clinical intervention.

Keywords Exosomal lncRNA, Mir100hg, ALDOA, Histone lactylation, H3K14

[†]Lei Shi, Bowen Li, Jiyu Tan and Ling Zhu contributed equally.

*Correspondence:

H. Rosie Xing

102643@cqmu.edu.cn

Jingyu Li

cqtnljy@hospital.cqmu.edu.cn

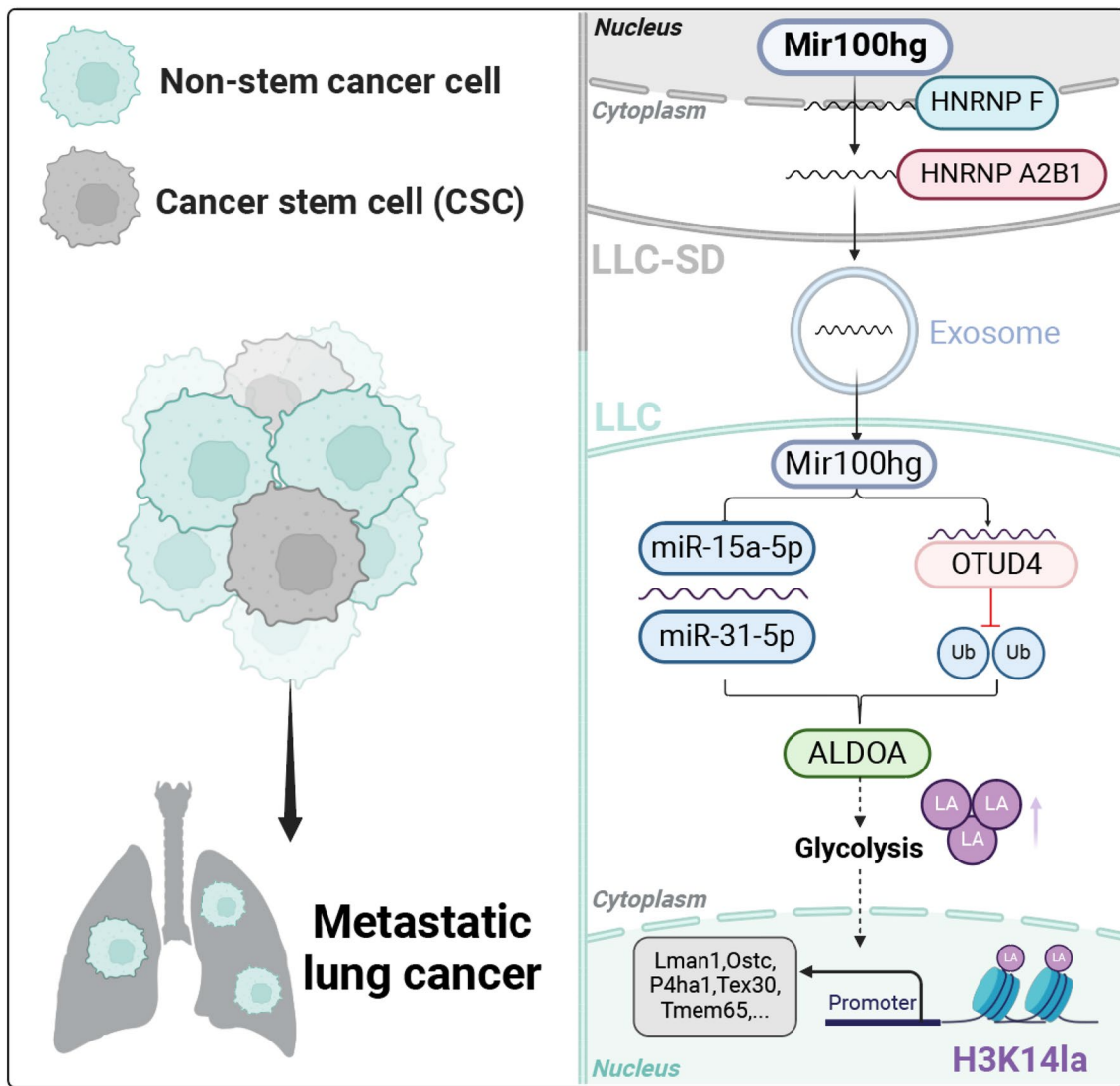
Jianyu Wang

102758@cqmu.edu.cn

Full list of author information is available at the end of the article



Graphical Abstract



Introduction

Lung cancer ranks first in both incidence and mortality among cancers. Late detection, high metastasis rate, high recurrence, and acquired resistance are the main reasons for its poor prognosis [1]. Cancer metastasis is a complex process. The mechanisms of interactions among heterogeneous cancer cells within the tumor microenvironment (TME) and metastatic microenvironment (MME), as well as their impact on tumor progression, awaits further in-depth research [2, 3]. The theory of cancer stem cells promoting oncogenesis and metastasis has been established [4]. To date, there are few reports on how they alter the communication between heterogeneous cancer cells

within the tumor [5]. Gaining new insights into the role of cancer stem cells in lung cancer metastasis may lead to the development of innovative therapeutic approaches to improve the prognosis of metastatic lung cancer patients.

The functionality and mechanisms of exosomes as mediators of cell–cell interactions have been extensively studied and have become a novel category of biomarkers in cancer diagnosis and prognosis [6, 7]. Recent studies have shown that exosomes can regulate the interaction between cells in the tumor microenvironment, particularly influencing the metastatic process through the transfer of their contents, especially non-coding RNAs [8]. While research has demonstrated the importance of

exosomal communication in tumor progression, there remains a significant knowledge gap regarding how CSCs utilize exosomes to influence the tumor microenvironment. Compared to miRNAs, the structure and mechanisms of action of long non-coding RNAs (lncRNAs) are more complex, involving multiple regulatory mechanisms and diverse molecular interactions [9]. Although research on lncRNAs has become a hot topic in cancer research in recent years [10], understanding of their roles in CSC-mediated tumor progression remains limited, particularly in the regulation of interactions between heterogeneous tumor cells [11, 12]. Additionally, the transport and packaging mechanisms of biologically active contents (such as non-coding miRNAs, lncRNAs) within exosomes (whether selective or regulated) remain unclear [13, 14], representing a critical knowledge gap in understanding how CSCs may exploit these mechanisms for tumor progression. Therefore, it is not yet known whether exosomal transport could be a novel intervention target for cancer treatment. Furthermore, there are few reports on the synergistic and efficient mechanisms by which exosomal lncRNAs reach target cancer cells and regulate their metastatic ability. Particularly, our understanding is limited regarding how these lncRNAs might simultaneously modulate multiple cellular processes, such as metabolism and transcriptional regulation, to promote metastasis. Thus, investigating the processes by which exosomes select and transport lncRNAs, along with the roles of these lncRNAs in recipient cells, is essential for the development of new therapeutic strategies aimed at targeting cellular communications.

Lactate, a primary by-product of glycolysis, is known to directly induce histone lactylation [15]. Lactylation is regarded as a vital link connecting cellular metabolic states and gene expression regulation [16]. This novel epigenetic modification is notably observed in environments with elevated lactate levels, particularly in tumor cells exhibiting increased glycolytic activity. Ma et al. investigated the impact of lactate on the cellular metabolism of non-small cell lung cancer (NSCLC) and found that elevated levels of lactate dehydrogenase (LDH) are associated with a poor prognosis in NSCLC. This suggests that lactate influences cellular metabolism in NSCLC, partly through gene expression mediated by histone lactylation [17]. Nonetheless, this research did not specify the precise mechanisms by which lactylation affects NSCLC. Liu et al. explored the impact of lactate-mediated histone modification on lncRNAs [18]. They showed that lipopolysaccharide (LPS) from bacteria could enhance LINC00152 expression by elevating histone lactylation levels at the lncRNA promoter, consequently promoting colorectal cancer progression. This provides novel insights into the regulatory mechanism of

histone lactylation on lncRNAs. However, the regulatory mechanisms of exosomal lncRNAs on metabolic reprogramming and histone lactylation in the tumor microenvironment remain unclear, particularly in both CSCs and non-CSCs.

The current study delves into the complex nature of lung cancer progression, with a specific focus on the regulatory network governing the exosomal secretion of long non-coding RNAs (lncRNAs) and its role in promoting lung cancer metastasis by facilitating interactions among heterogeneous tumor cells. Notably, the findings of this study highlight the multifaceted role of Mir100hg in lung cancer metastasis. Importantly, the research establishes a connection between metabolic reprogramming and epigenetic regulation, elucidating the molecular mechanisms underlying the role of exosomal lncRNAs in lung cancer progression. Furthermore, the identification of ALDOA and histone lactylation as key components in this regulatory network provides valuable insights into potential therapeutic targets for lung cancer treatment, particularly in the context of exosomal communication and epigenetic modifications. These findings contribute to a deeper understanding of lung cancer biology and may pave the way for the development of novel therapeutic strategies targeting exosomal lncRNAs and histone lactylation pathways.

Methods

Cell lines and culture

In the present study, we used the lung adenocarcinoma cell line Lewis lung carcinoma (LLC) and CSC-like Lewis lung carcinoma cells (LLC-SD) that we previously reported, which were isolated and purified from the parent LLC cells [19]. LLC cells were maintained in DMEM high glucose (Gibco, USA) supplemented with 10% fetal bovine serum (FBS) (Gibco, USA) and 1% penicillin–streptomycin (Hyclone, USA). LLC-SD cells were cultured in DMEM/F12 (Hyclone, USA) with the addition of 1% B27 (Gibco, USA) and 1% penicillin–streptomycin (Hyclone, USA).

Exosome extraction and characterization

Upon reaching 90% confluence, LLC-SD cells were processed via differential centrifugation to collect the supernatant for exosome extraction. This process involved: centrifugation of the supernatant at 800×g for 5 min at 4 °C, followed by further centrifugation of the samples at 10,000×g for 45 min at 4 °C. Subsequently, centrifugation was performed at 2000×g for 10 min at 4 °C using a 100 kDa MWCO (Millipore, USA) centrifugal concentrator. The supernatant was then centrifuged at 100,000×g for 70 min at 4 °C, and the supernatant was discarded. The exosome precipitate was washed in 2 mL PBS and

centrifuged once again at 100,000×g for 70 min at 4 °C. The final exosome precipitate was resuspended in 200–300 µL PBS and stored at – 80 °C. Transmission electron microscopy (TEM; JEM-1400PLUS, JEOL) was used to analyze the morphology of exosomes. Nanoparticle tracking analysis (NTA) was used to determine the size distribution and concentration of exosomes. The TEM and NTA characterization results were supported by Beijing Zhongkebaice Technology Service Co., Ltd. Western blot (WB) was employed to characterize and identify the exosome markers.

Exosomes labeling and tracing

Following extraction and purification, PKH26 red fluorescent labeling stain (PKH26, Umibio Co., Ltd, Shanghai) was thoroughly mixed with the exosomes and incubated in the dark for 10 min. Next, PKH26-labeled exosomes (100 µg) were added to the cultured LLC cells and then collected at the indicated time points (1 h/2 h/3 h). Plates were gently washed twice with PBS, then fixed in ice-cold methanol for 30 min at 4 °C. Cells were stained with 10 µL of DAPI nuclear dye for 10 min at 37 °C in the dark. Images were acquired using a confocal fluorescence microscope (ANDOR, Dragonfly200).

RNA nucleoplasmic isolation

Cytoplasmic and nuclear RNA isolation was conducted with the Cytoplasmic & Nuclear RNA Purification Kit (Norgen Biotek). Cells were harvested and transferred into 1.5 mL centrifuge tubes with 200 µL of ice-cold Lysis Buffer J for cell lysis. The lysate was then centrifuged at 12,000g for 10 min using a benchtop centrifuge. While the supernatant contained the cytoplasm contents, the insoluble precipitate was the content of the nucleus. A column wash was performed to purify the RNA. The RNA was then eluted into a new 1.7 mL elution tube. This was followed by reverse transcription and qRT-PCR.

RNA immunoprecipitation (RIP)

RIP was carried out with the PureBinding® RNA Immunoprecipitation Kit (Genesee Biotech Co., Ltd., P0102, Guangzhou, China). Following cell lysis, A/G magnetic beads were conjugated with IgG or specific RIP protein antibodies, respectively and incubated overnight at 4 °C. Purified RNA–protein complexes were subsequently analyzed using real-time PCR and WB.

Full-length lncRNA amplification

Following total RNA extraction, reverse transcription into cDNA was performed, with subsequent design of specific primers for the target lncRNA synthesis. For the full-length RNA synthesis, 25 µL of Taq mix, 5 µL of cDNA, 4 µL of primer, and 16 µL of ddH₂O were added

for PCR amplification. The amplification program was set as the following: denaturing at 95 °C for 3 min, followed by 95 °C for 15 s, and 35 cycles of amplification at 58 °C for 15 s and primer extension at 72 °C for 80 s, completing with 72 °C for 5 min. and Electrophoresis was conducted at 150 V for 50 min. Post-electrophoresis, the size of RNA species was assessed by UV illumination. A gel recovery kit (YiSEN) was utilized to purify the identified PCR product as a template for transcription, yielding the target RNA. RNA synthesized in vitro was labeled with biotin (APEX BIO, Houston, USA) and subsequently purified for future applications.

RNA-pulldown assays (RNA-PULLDOWN)

RNA-pulldown assays were performed using the PureBinding® RNA–Protein pull-down Kit (Genesee Biotech Co., Ltd., P0201, Guangzhou, China). 50 µL streptavidin magnetic beads were added to a 1.5 mL EP tube. The supernatant was discarded after placing the tube on a magnetic rack. The beads were washed with an equal volume of 20 mM Tris buffer and then vortexed. An equal volume of 1 × RNA capture buffer was then added and the magnetic beads were resuspended again by vortexing. 50 pmol (17 µg) of labeled RNA was added and gently mixed using a pipette. Incubation with rotation was carried out for 15–30 min at room temperature. The tube was then placed on a magnetic rack and the supernatant discarded. The beads were washed with an equal volume of 20 mM Tris buffer and placed back on the magnetic rack to discard the supernatant. The 10 × Protein-RNA Binding Buffer was diluted to 1 ×, and 100 µL of this buffer was added to the EP tubes containing the magnetic beads and thoroughly mixed. A premix solution for the RNA–protein binding reaction was prepared. The tube was placed on a magnetic rack, and supernatant A was collected after adding 100 µL of Master Mix to release the bound RNA. The beads were then washed with 100 µL of 1 × wash buffer, placed on the magnetic rack, and supernatant B was collected. 50 µL of Elution Buffer was added to the magnetic beads and thoroughly vortexed. Incubation with rotation occurred at 37 °C for 15–30 min. After placing the tube on a magnetic rack, the supernatant was discarded. The eluted samples were heated at 95–100 °C for 5–10 min. Samples were processed immediately or stored at – 20 °C until further use.

Immunofluorescence

Cells were seeded onto confocal dishes, and when the confluence reached 70–80%, the medium was removed, and the cells were fixed with paraformaldehyde for 30 min at room temperature. Cell membrane permeabilization was achieved using 0.2% Triton X-100 at 4 °C for 20 min. Blocking was performed with 2% BSA for

one hour. Incubation with the primary antibody mixture occurred overnight at 4 °C. Following this, the secondary antibody mixture was incubated in darkness at 37 °C for 1 h. DAPI staining was conducted for 10 min at room temperature. Slides were sealed with a fluorescence quenching agent and stored in darkness. Images were acquired using a confocal fluorescence microscope (ANDOR, Dragonfly200).

Fluorescence in situ hybridization (FISH)

Cells were seeded onto the 24-well plates, let grow to 70% confluence, and then fixed with 4% paraformaldehyde for 10 min at room temperature. This was followed by permeabilization with 1% Triton X-100 and blocking with 5% BSA for 1 h at room temperature. Cy3-labeled lncRNA-Mir100hg was incubated with the cells overnight at 37 °C. The next day, cells were washed three times with PBS and nuclei were stained with DAPI (Sigma-Aldrich, USA) in darkness. The cell slides were mounted using transparent resin, and a drop of anti-fluorescence quenching agent was applied before storing in darkness. Images were acquired using a confocal fluorescence microscope (ANDOR, Dragonfly200).

Dual luciferase reporter assay

Mir100hg wild type reporter plasmid and mutant reporter plasmid of ~500 bp upstream and downstream of the miRNAs potential binding site were synthesized by HanBio Tech (Shanghai, China). After cloning into the psiCHECK-2 polyclonal site, the plasmid was co-transfected with the mimics/NC of miRNA into 293 T cells, and the luciferase activity was measured 48 h later.

Animal experiments

All animal experiments were conducted following the National Institutes of Health (NIH Publication No. 85-23, revised 1996) Guidelines for the Care and Use of Laboratory Animals. The studies were approved by the Chongqing Medical University Ethics Committee (#SCXK2022-0010) and reviewed by Chongqing Medical University's Committee for the Management and Use of Laboratory Animals (IACUC-CQMU). Male NOD-SCID mice, 7–8 weeks old, used in this study were obtained

from Chongqing Enswell Animal Company. Randomization ensured equal mean weights of mice in each group. 5×10^5 cells were injected into each mouse's tail vein, and body weights were recorded every three days. Animals experiencing continuous weight loss for one week were humanely euthanized by cervical dislocation. Following gross dissection, a Salestromz87 fluorescent imager (LUYOR, 3430-RB, Shanghai) was employed to observe tumor colonization and metastasis.

Statistical analyses

All experiments were repeated to obtain three independent biological replicas. Data are expressed as means \pm standard error of the mean (SEM). Differences between means were evaluated using the Student's t-test or Wilcoxon rank sum test. Asterisks indicate significant differences as follows: * $P < 0.05$, ** $P < 0.01$, and *** $P < 0.001$.

A detailed description of the Materials and Methods used in this study can be found in Supplementary Files.

Results

HNRNPF interacts with Mir100hg and promotes its translocation from the nucleus to the cytoplasm in CSCs

Our previous study revealed that exosomes from LLC-SD enhance the metastatic colonization capability of LLC both in vitro and in vivo [20]. Here, we observed higher expression of Mir100hg in LLC-SD compared to LLC cells (Fig. S1A). Knocking down Mir100hg in LLC-SD cells resulted in decreased levels of Mir100hg in the derived exosomes (LLC-SD-Exo) (Fig. S1B, C). LLC-SD-Exo was characterized via Western blot, NTA, and electron microscopy (Fig. S1D–F). After co-culturing LLC-SD-Exo with LLC cells, the exosomes from the Mir100hg knockdown group significantly lost their ability to promote migration and invasion (Fig. S1G). Using the mouse tail vein lung metastasis model, the LLC-SD-sh-Mir100hg-Exo group exhibited fewer metastases in the lungs, heart, and chest wall, and less weight loss compared to the control group (Fig. 1A, B; S1H–J). These results suggest that Mir100hg plays a critical role in the oncogenic effect of LLC-SD-Exo.

(See figure on next page.)

Fig. 1 HNRNPF interacts with Mir100hg and promotes its localization within the cytoplasm. **A** Schematic diagram of exosome-based animal experiments; **B** Fluorescence imaging of mouse lung tumor (green) and hematoxylin and eosin (HE) stained lung section; **C** Nucleoplasmic RNA isolation from LLC and LLC-SD cells; **D** Fluorescence in situ hybridization (FISH) of Mir100hg in LLC and LLC-SD cells; **E** RNA pulldown assay for Mir100hg; **F** Venn diagram of RNA pulldown results; **G** Table of information related to HNRNP family protein profiles in RNA-pulldown results; **H** Nuclear and cytoplasmic RNA isolation from LLC-SD after knocking down HNRNP family proteins; **I** FISH analysis of Mir100hg; **J** RNA immunoprecipitation (RIP) for Mir100hg and HNRNPF; **K** RNA pulldown for Mir100hg and HNRNPF; **L** Fluorescence co-localization of Mir100hg and HNRNPF. **M** Schematic representation of direct binding of Mir100hg to HNRNPF for nucleoplasmic translocation. (* $p < 0.05$, ** $p < 0.01$, *** $p < 0.001$)

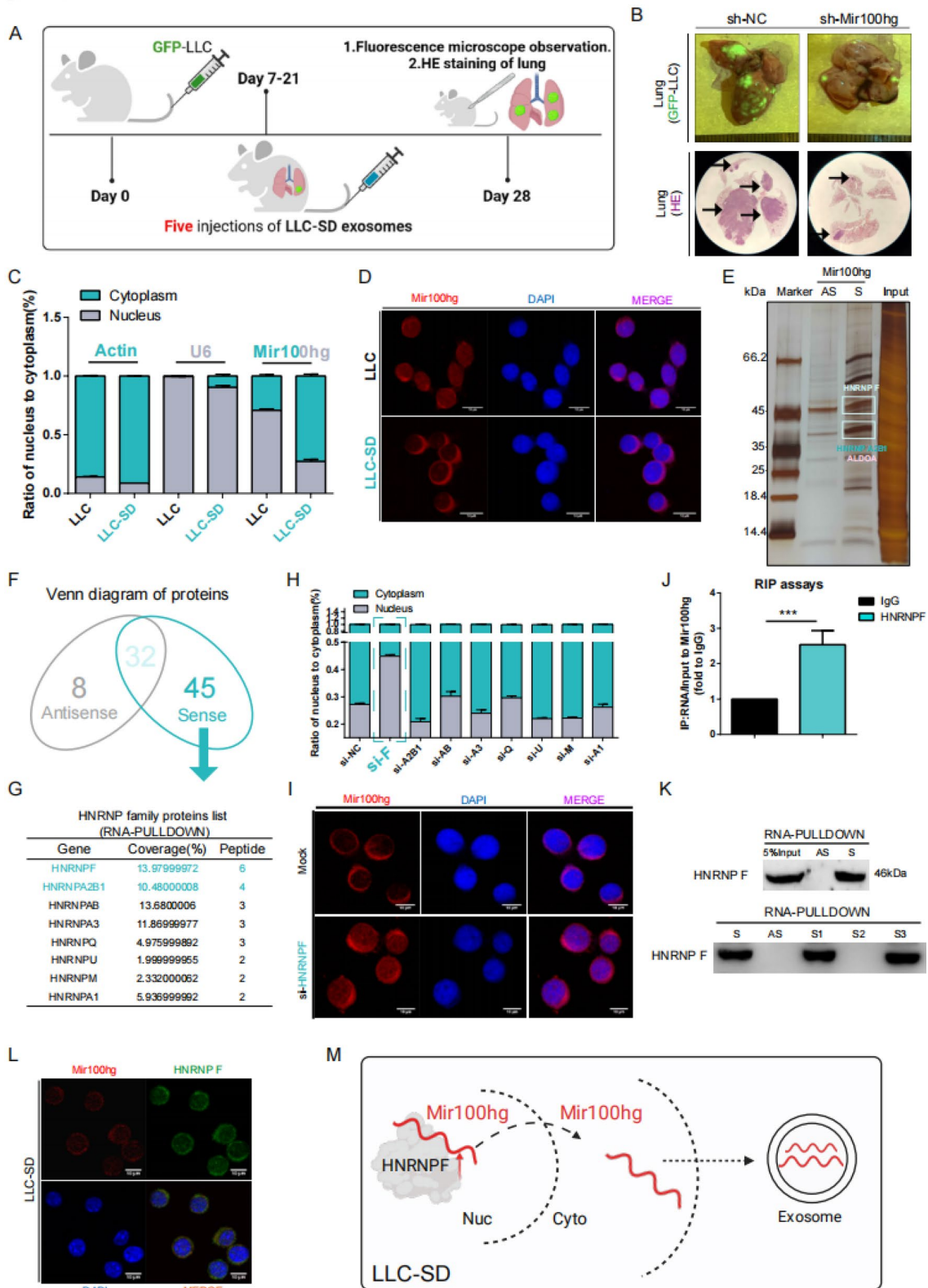


Fig. 1 (See legend on previous page.)

Several studies have demonstrated that Mir100hg is primarily localized in the nucleus, regulating transcription through either in a cis- or trans- manner [21–23]. Intriguingly, Mir100hg displayed distinct localization in LLC-SD and LLC cells, with primarily cytoplasmic localization in LLC-SD and nuclear localization in LLC (Fig. 1C, D). To investigate the factors contributing to the distinct nucleoplasmic localization of Mir100hg, RNA pull-down assay (RNA-PULLDOWN) was conducted (Fig. 1E). Forty-five proteins bound to Mir100hg were identified, mainly involved in localization and transporter pathways (Fig. 1E, F, Fig. S2A, B; Supplementary Table 1). Many of these proteins belong to the hnRNP family (Fig. 1G). Analysis of The Cancer Genome Atlas-Lung Adenocarcinoma (TCGA-LUAD) database revealed significantly higher levels of these hnRNP proteins in lung adenocarcinoma patients compared to the non-tumor group (Fig. S2C). High HNRNPF and HNRNPA2B1 expression correlated with reduced overall survival (Fig. S2D).

To ascertain whether hnRNP family proteins mediate the nucleoplasmic translocation of Mir100hg, we silenced HNRNPs in LLC-SD cells using small interfering RNA (siRNA) (Fig. S2E) and evaluated changes in Mir100hg localization. Silencing HNRNPF significantly altered Mir100hg localization, increasing nuclear and decreasing cytoplasmic levels (Fig. 1H), confirmed by FISH results (Fig. 1I). Analysis of the mass spectrometry results of HNRNPF in MIR100HG-pulldown (Fig. S2F), coupled with RNA immunoprecipitation (RIP), RNA-pulldown assays, Immunofluorescence co-localization and molecular docking simulations, confirmed a direct interaction between HNRNPF and Mir100hg (Fig. 1J–L; Fig. S2G). The predicted secondary structure of Mir100hg was used in the RNA pull-down assay (Fig. S2H–J). The results showed high binding affinity between Mir100hg and HNRNPF in the S1 (1-1247nt) and S3 (2155-3022nt) fragments (Fig. 1K). Collectively, these findings indicate that HNRNPF enhances the cytoplasmic localization of Mir100hg through direct interaction, possibly leading to increased Mir100hg levels in the exosomes of lung cancer stem cells, thereby enhancing the metastatic potential of non-stem cancer cells.

HNRNPA2B1 enhances the metastatic potential of LLC by facilitating the incorporation of Mir100hg into exosomes

To confirm the exosomal transfer of Mir100hg from LLC-SD to LLC, a Cy5-Biotin-Mir100hg tracing experiment was conducted (Fig. 2A). Reverse transcription polymerase chain reaction (RT-PCR) and confocal microscopy verified its transfection into LLC-SD cells (Fig. S3A, B). Following co-culture of LLC-SD-Exo with LLC cells, exogenous Mir100hg was observed in LLC cytoplasm (Fig. 2B), with increased expression of Mir100hg in LLC cells (Fig. 2C), indicating the infiltration of LLC-SD exosomal Mir100hg into LLC cells. HNRNP silencing, particularly HNRNPA2B1, resulted in reduced Mir100hg levels in exosomes, suggesting its role in regulating the entry of Mir100hg into exosomes (Fig. 2D). Mass spectrometry, molecular docking, RIP, and RNA-PULLDOWN confirmed the direct binding between HNRNPA2B1 and Mir100hg (Fig. 2E, F; Fig. S3C, D), with a strong affinity for S1 (1-1247nt) and S2 (1247-2155nt) fragments (Fig. 2F). FISH and immunofluorescence assays showed colocalization of Mir100hg and HNRNPA2B1 in LLC-SD cells (Fig. S3E). Silencing HNRNPA2B1 in LLC-SD cells significantly reduced the level of Mir100hg in exosomes (Fig. 2G; Fig. S3F, G). Co-culturing of LLC cells with exosomes from sh-HNRNPA2B1-LLC-SD and sh-NC-LLC-SD showed that HNRNPA2B1 silencing in LLC-SD cells reduced Mir100hg levels in recipient LLC cells (Fig. 2H) and significantly diminished their migration and invasion capability in vitro (Fig. 2I, J). Additionally, concomitant silencing of HNRNPA2B1 and HNRNPF in LLC-SD cells significantly reduced the migration and invasion of co-cultured LLC cells (Fig. S3H). These findings indicate that the pro-metastatic effect of LLC-SD-Mir100hg on LLCs is dependent on HNRNPA2B1-mediated entry of Mir100hg into the exosomes.

Mir100hg promotes the metastasis of lung cancer cells in vitro and in vivo by up-regulating ALDOA expression

Cancer development and progression involve metabolic shifts in cells to support its rapid growth [24]. To identify key metabolic regulators downstream of Mir100hg, we performed RNA-PULLDOWN coupled with mass

(See figure on next page.)

Fig. 2 HNRNPA2B1 enhances the metastatic potential of LLC by facilitating the incorporation of Mir100hg into exosomes. **A** Schematic diagram of exosomal Mir100hg tracing experiment; **B** Co-localization of Mir100hg and exosomes in LLC cells; **C** Bar graph showing differential expression of Mir100hg in LLC cells post-exosome incubation; **D** Mir100hg expression in LLC-SD exosomes following HNRNP family protein knockdown; **E** RNA immunoprecipitation (RIP) for Mir100hg and HNRNPA2B1; **F** RNA pull-down for Mir100hg and HNRNPA2B1; **G** Mir100hg expression in LLC-SD cells following HNRNPA2B1 knockdown; **H** Mir100hg expression in LLC cells co-cultured with exosomes from HNRNPA2B1-knockdown LLC-SD cells; **I, J** Transwell for LLC cells post-co-culture with LLC-SD exosomes and the counting chart. (* $p < 0.05$, ** $p < 0.01$, *** $p < 0.001$)

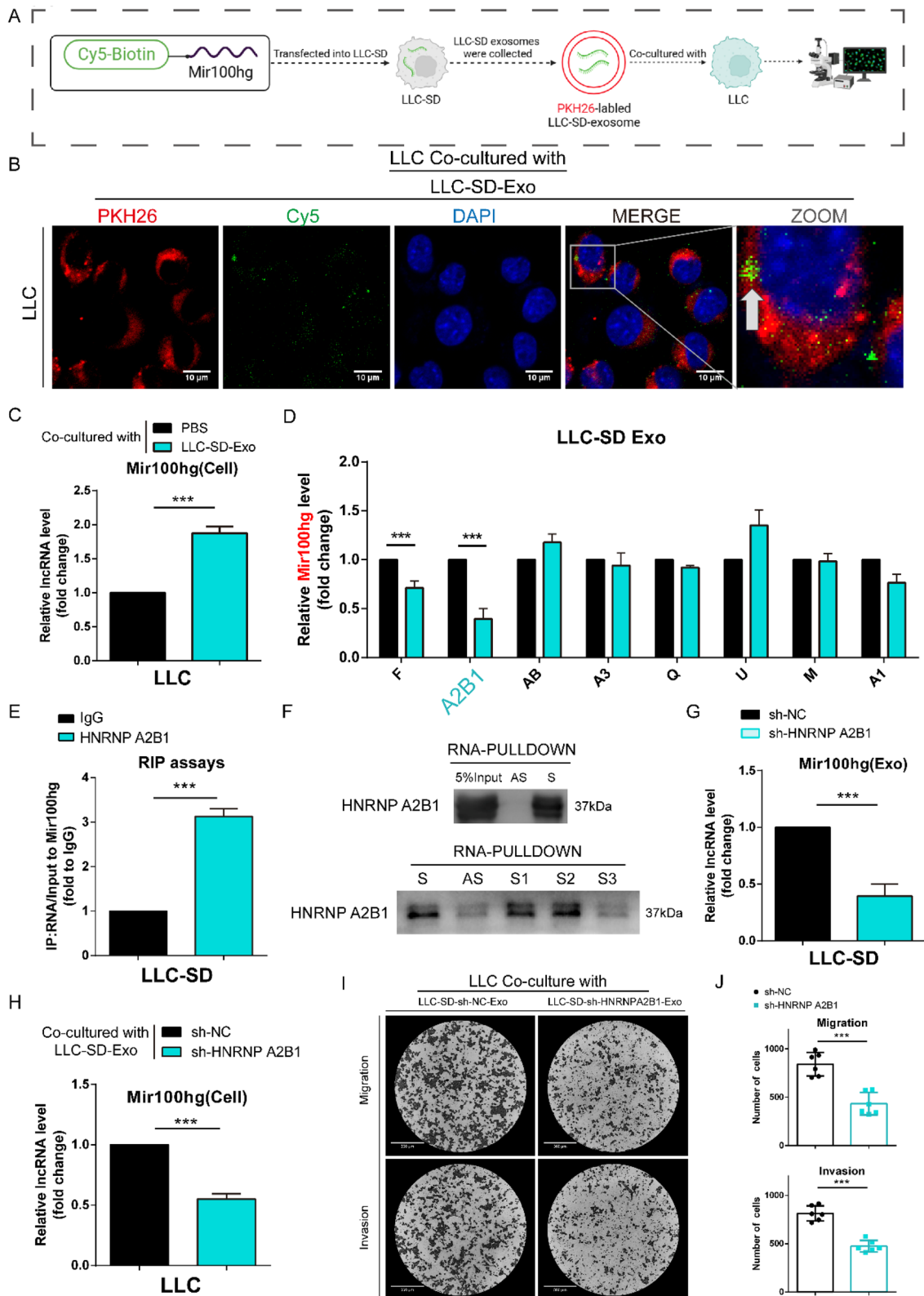


Fig. 2 (See legend on previous page.)

spectrometry analysis, which highlighted aldolase A (ALDOA) as the only glycolysis-related protein among Mir100hg-interacting proteins (Fig. 3A). ALDOA functions as a rate-limiting enzyme in glycolysis, and our analysis of TCGA database revealed its significant overexpression in lung adenocarcinomas compared to non-tumor tissues, with high expression correlating with reduced patient survival (Fig. 3B, C). These findings led us to hypothesize that Mir100hg promotes lung cancer metastasis by upregulating ALDOA, thereby enhancing glycolysis. We demonstrated that ALDOA expression is positively correlated with Mir100hg expression (Fig. 3D). Overexpression of Mir100hg (OE-Mir100hg) enhanced the migration and invasion ability of lung cancer cells, while knockdown of ALDOA in OE-Mir100hg-LLC significantly reversed this phenotype (Fig. 3E, F). The mouse tail vein model and hematoxylin and eosin (HE) staining results also showed a similar trend (Fig. 3G, H). These results suggest that Mir100hg enhances the metastatic ability of lung cancer cells in an ALDOA dependent manner. ALDOA is well-known for its role in catalyzing the conversion of Fructose-1,6-bis-phosphate (FBP) into Dihydroxyacetone Phosphate (DHAP) and Glycerinaldehyde-3-phosphate (GADP) in glycolysis (Fig. 3I). To investigate whether Mir100hg involving ALDOA affects downstream metabolic processes, GADP was added to ALDOA knockdown cells. We observed that GADP could restore the reduced migration and invasion abilities caused by ALDOA knockdown (Fig. 3J). These results indicate that Mir100hg enhances the migration and invasion ability of lung cancer cells, dependent on the glycolysis process involving ALDOA.

Mir100hg positively regulates ALDOA mRNA and protein levels through CeRNA and OTUD4-deubiquitination

It is well-established that lncRNAs can function as scaffolds, influencing the ubiquitination of the bound proteins [25–28]. Molecular docking, RIP, and RNA-PULLDOWN (Fig. 4A, B; Fig. S4A) confirmed the direct binding between ALDOA and Mir100hg, with the S1/S3 fragment showing stronger interaction. The use of MG132, a proteasome inhibitor, can inhibit the positive regulation of ALDOA by Mir 100hg, suggesting that Mir100hg may regulate ALDOA through

proteasomal degradation (Fig. 4C). To further validate the role of Mir100hg in post-translational regulation of ALDOA degradation, cells were treated with the protein synthesis inhibitor cycloheximide (CHX). Results showed a faster decrease in ALDOA protein levels in Mir100hg silencing (sh-Mir100hg) cells than in controls, while Mir100hg overexpression (OE-Mir100hg) delayed ALDOA degradation following CHX treatment (Fig. 4D). We subsequently investigated whether ubiquitination is involved in the Mir100hg-dependent degradation of ALDOA. Immunoprecipitation analysis revealed an inverse correlation between Mir100hg expression and ALDOA ubiquitination (Fig. 4E). These findings confirm that Mir100hg enhances ALDOA stability through the ubiquitin–proteasome system. To unravel the mechanism by which Mir100hg regulates the ubiquitin–proteasome degradation of ALDOA, we conducted ALDOA pull-down assays and identified OTUD4, a deubiquitinase (Fig. 4F; Supplementary Table 2). The OTU family, as a major deubiquitinating enzyme group, is crucial for DNA repair, immune response, metabolic balance, and tumor development [29–33]. Thus, we hypothesized that OTUD4 may promote ALDOA deubiquitination. Silencing OTUD4 in OE-Mir100hg cells significantly increased ALDOA ubiquitination (Fig. 4G; Fig. S4B). We further investigated whether Mir100hg regulates the interaction between ALDOA and OTUD4. Following Mir100hg silencing, there was a decrease in OTUD4 protein co-precipitating with ALDOA compared to control cells (Fig. 4H), while Mir100hg-overexpression resulted in increased co-precipitation of OTUD4 with ALDOA (Fig. 4I). Furthermore, RIP and RNA-PULLDOWN experiments confirmed the strong and direct binding of the S1/S2 fragment of Mir100hg to OTUD4 (Fig. 4J, K). Immunofluorescence and FISH experiments revealed co-localization of Mir100hg, OTUD4, and ALDOA in the cytoplasm (Fig. 4L). Transwell assays demonstrated that OTUD4 knockdown in OE-100 cells significantly reduced lung cancer cell migration and invasion in vitro (Fig. S4C, D). These findings suggest that Mir100hg recruits deubiquitinase OTUD4 to the ALDOA protein, thus impeding its degradation via the ubiquitin–proteasome system (Fig. 4M).

(See figure on next page.)

Fig. 3 Mir100hg promotes the metastasis of lung cancer cells in vitro and in vivo by up-regulating ALDOA expression. **A** Protein profile of ALDOA in RNA-PULLDOWN; **B** ALDOA expression differences in TCGA-LUAD database; **C** Line graph of the effect of ALDOA on overall survival in TCGA-LUAD database; **D** Analysis of ALDOA protein levels in Mir100hg knockdown (sh-Mir100hg) and overexpression cells (OE-Mir100hg); **E, F** Transwell of the migration and invasion ability of LLC cells and the counting chart; **G** Lung tumors in various mouse groups (green); **H** Hematoxylin and eosin (HE) stained lung sections (arrows indicate tumor areas); **I** Schematic diagram of ALDOA involvement in glycolysis; **J** Transwell migration and invasion assays post-addition of GADP in ALDOA knockdown cells and the counting chart. (* $p < 0.05$, ** $p < 0.01$, *** $p < 0.001$)

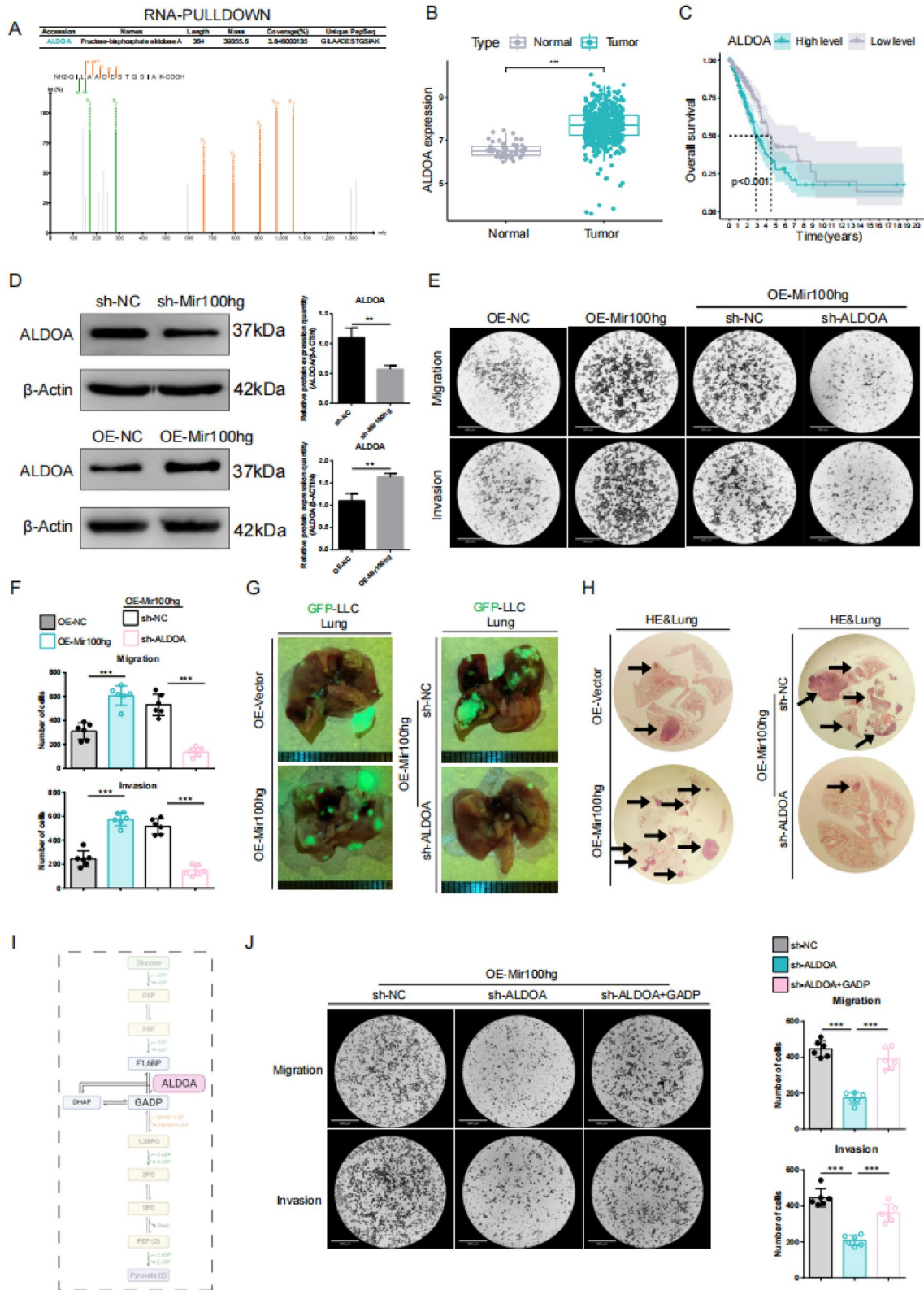


Fig. 3 (See legend on previous page.)

Our previous study demonstrated that Mir100hg targets two miRNAs, miR-15a-5p and miR-31-5p, via the competitive endogenous RNA (CeRNA) regulation mechanism, thereby promoting lung cancer metastasis [20]. We hypothesized that Mir100hg may not only directly influence ALDOA expression through protein stability but also modulates its mRNA levels via miR-15a-5p and miR-31-5p. In OE-Mir100hg group, a decrease in miR-15a-5p/miR-31-5p expression and increased Aldoa mRNA levels were observed (Fig. S4E), while knockdown of Mir100hg led to elevated miR-15a-5p/miR-31-5p expression and reduced Aldoa mRNA levels (Fig. S4F). Additionally, simultaneous overexpression of miR-15a-5p and miR-31-5p in OE-Mir100hg-LLC cells significantly inhibited Aldoa mRNA levels, while their suppression in sh-Mir100hg-LLC cells increased Aldoa mRNA levels (Fig. S4G, H). These findings confirm the molecular relationships of the transcriptional axis that involves the CeRNA network of Mir100hg, miR-15a-5p, miR-31-5p, and Aldoa. We then constructed dual-luciferase reporter systems for both the wild-type and mutant plasmids of ALDOA (Fig. S4I). The reduction in luminescence intensity in cells transfected with Mir100hg-WT and Aldoa-WT plasmids indicates that these microRNAs can directly target ALDOA. Importantly, the lack of significant change in luminescence intensity when mutations were introduced at the corresponding binding sites suggests that Mir100hg's interaction with ALDOA is mediated by sequestering miR-15a-5p and miR-31-5p, preventing them from binding to ALDOA (Fig. S4J). These results support our hypothesis that Mir100hg binds to ALDOA and modulates its expression through sequestration of miR-15a-5p and miR-31-5p. To further confirm the inhibitory effect of direct targeting of ALDOA by miR-15a-5p and miR-31-5p on the metastatic potential of lung cancer cells, we suppressed miR-15a-5p and miR-31-5p in wild-type LLC cells (Fig. S4K), which resulted in increased ALDOA expression (Fig. S4L). Subsequent Transwell assays revealed that simultaneous suppression of miR-15a-5p and miR-31-5p significantly enhanced the migratory and invasive capabilities of LLC cells, whereas knockdown

of ALDOA led to a noticeable reduction in these capabilities (Fig. S4M). Importantly, we observed that GADP could restore the reduced migration and invasion abilities caused by overexpressing miR-15a-5p and miR-31-5p (Fig. S4N). This suggests that the downstream effects of the CeRNA network regulated by Mir100hg are likely dependent on the glycolytic process involving ALDOA.

Taken together, these findings suggest that Mir100hg positively regulates ALDOA expression through CeRNA and OTUD4-mediated deubiquitination, which subsequently enhances the migration and invasion of lung cancer cells.

Mir100hg facilitates lung cancer cell metastasis by enhancing histone lactylation

Metabolomic analysis demonstrated a significant increase in intracellular lactate production following Mir100hg overexpression (Fig. 5A), suggesting that Mir100hg positively regulates lactate generation in lung cancer cells. Additionally, utilizing Fila-Nuc, a recognized lactate sensor [34], we observed a significant elevation in nuclear lactate levels in OE-Mir100hg cells compared to the control group (Fig. S5A). Since lactate serves as the substrate for histone lactylation [15], we posit that Mir100hg may play a role in the regulation of histone lactylation in lung cancer cells. Western blot and immunofluorescence assays revealed a significant increase in histone lactylation levels, notably at H3K9, H3K14, H3K18, and H4K16, with the most pronounced increase observed at H3K14 in OE-Mir100hg cells (Fig. 5B–D; Fig. S5B, C). Consequently, we focused further investigation on the effect of Mir100hg on H3K14 lactylation.

To validate the impact of glycolysis and histone lactylation on lung cancer cell functions, we employed the glucose and glycolysis inhibitor 2-deoxy-D-glucose(2-DG), along with lactate dehydrogenase A inhibitor GNE140 (GNE) and sodium lactate (Nala) (Fig. 5E). The findings indicate that glucose significantly enhanced the migration and invasion capabilities of lung cancer cells (Fig. S5D), whereas 2-DG notably reduced their metastatic potential (Fig. S5E). These results strongly suggest that glycolysis plays a crucial role in augmenting the

(See figure on next page.)

Fig. 4 Mir100hg positively regulates ALDOA mRNA and protein levels through CeRNA and OTUD4-deubiquitination. **A** RNA immunoprecipitation (RIP) for Mir100hg and ALDOA; **B** RNA pulldown for Mir100hg and ALDOA; **C** Analysis of ALDOA protein levels post-MG132 treatment in Mir100hg knockdown and overexpression cells; **D** Analysis of ALDOA protein levels and relative band intensity quantification at indicated time points post-CHX treatment in Mir100hg knockdown and overexpression cells; **E** Ubiquitination levels of pulldown ALDOA protein analyzed by Western blot in Mir100hg knockdown and overexpression cells; **F** Protein spectrum results for OTUD4; **G** Ubiquitination analysis of ALDOA protein pulldown in OTUD4 knockdown cells by Western blot; **H, I** Analysis of OTUD4 levels following ALDOA protein pulldown in Mir100hg knockdown cells and Analysis of OTUD4 levels following ALDOA protein pulldown in Mir100hg knockdown cells; **J, K** RNA immunoprecipitation (RIP) and RNA-PULLDOWN for Mir100hg and OTUD4; **L** Fluorescence co-localization of Mir100hg with OTUD4 and ALDOA; **M** Schematic representation of ALDOA ubiquitination inhibition by Mir100hg through OTUD4 (* $p < 0.05$, ** $p < 0.01$, *** $p < 0.001$)

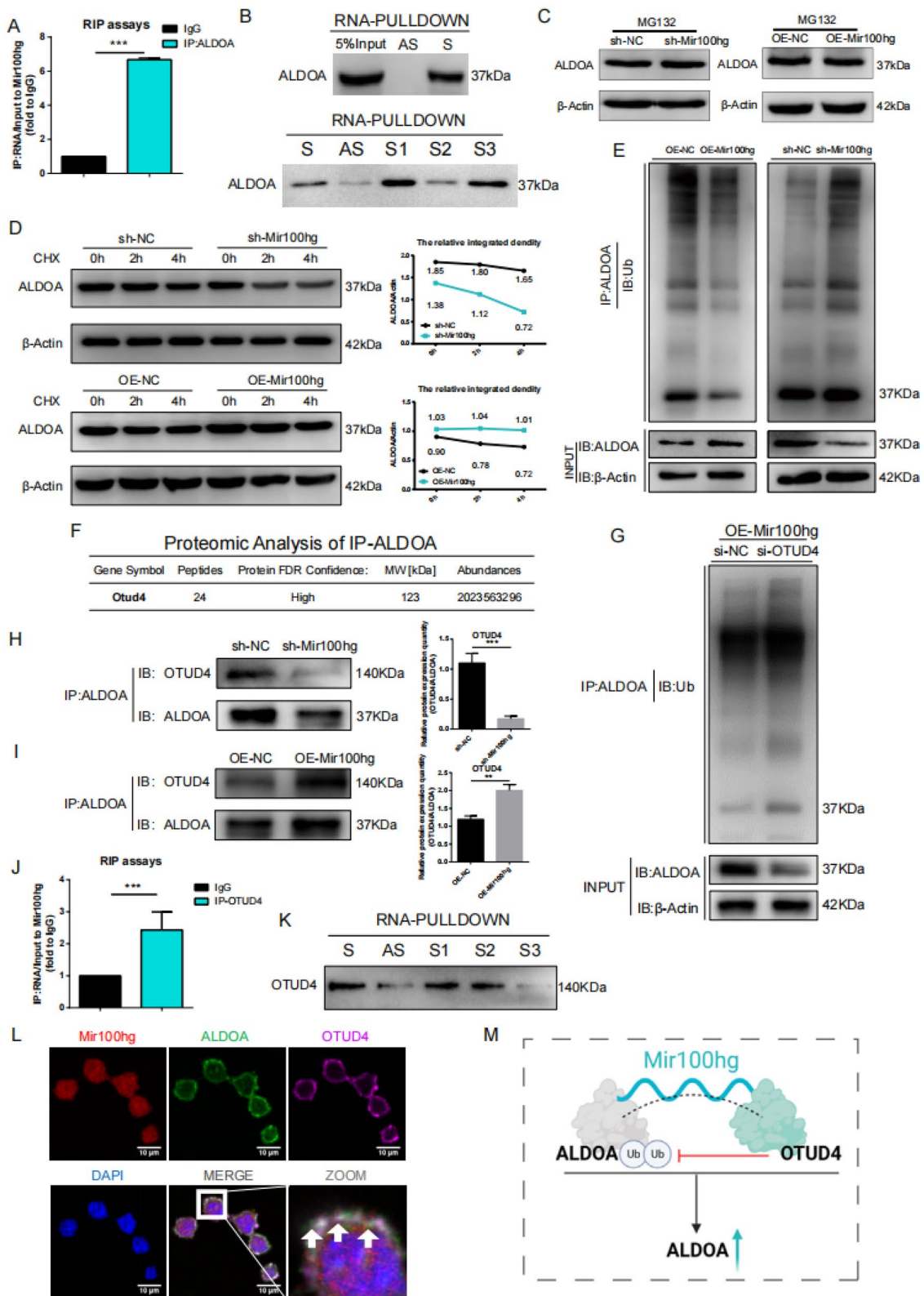


Fig. 4 (See legend on previous page.)

metastatic and invasive capacities of lung cancer cells. Additionally, a significant reduction in global and H3K14 lactylation levels was observed in lung cancer cells after GNE treatment (Fig. S5F), whereas Nala treatment led to increases in these levels (Fig. S5G). Furthermore, in OE-Mir100hg cells, GNE reduced both global and H3K14 lactylation, which was effectively reversed by Nala (Fig. 5F). Transwell experiments demonstrated that lactylation inhibition induced by GNE attenuated lung cancer cell migration and invasion *in vitro* (Fig. S5H), whereas Nala treatment increased their metastatic potential (Fig. S5I). Notably, in the OE-Mir100hg group, GNE or si-Ldha reduced both migration and invasion, effects that were reversed by Nala (Fig. 5G, H).

Taken together, these findings suggest that Mir100hg enhances both global and H3K14 lactylation in lung cancer cells, thereby contributing to lung cancer metastasis.

H3K14 lactylation enhances the expression of genes associated with lung cancer metastasis

To investigate the role of H3K14 lactylation in lung cancer, four experimental groups were established: OE-NC, OE-Mir100hg, OE-Mir100hg with GNE treatment (GNE), and GNE treatment followed by Nala recovery (GNE+NALA). Cleavage under targets and tagmentation (CUT&Tag) was employed to generate genome-wide H3K14la histone modification maps. The analysis of genomic coverage revealed elevated H3K14la modification in the OE-Mir100hg and GNE+NALA groups, primarily enriched at the promoter regions (Fig. 6A), with typical sharp peaks confined to transcription start site (TSS) (Fig. 6B). RNA-Seq and CUT&Tag data showed the highest H3K14la enrichment at promoter regions in the top 25% expressed genes, with a progressive decrease observed in lower quartiles, suggesting a positive correlation between H3K14la and mRNA expression levels (Fig. 6C). We analyzed Assay for Transposase-Accessible Chromatin sequencing (ATAC-Seq) data from GEO and found that genes with H3K14la enrichment in promoter exhibited higher chromatin accessibility in lung cancer, indicating that H3K14la regulates transcription by establishing chromatin accessibility (Fig. 6D). We hypothesized that Mir100hg promotes lung cancer cell metastasis by enhancing H3K14la-triggered gene transcription. RNA sequencing (RNA-Seq) and CUT&Tag

data from the OE-Mir100hg and control groups revealed that upregulated genes in OE-Mir100hg group exhibited higher H3K14la accumulation at promoter regions (Fig. 6E). Gene set enrichment analysis (GSEA) analysis (Fig. 6F) revealed significant enrichment of tumor metastasis-related genes in the OE-Mir100hg group, with 63% of the upregulated genes displaying H3K14la enrichment (Fig. 6G). Kyoto Encyclopedia of Genes and Genomes (KEGG) analysis of these genes suggested a close association with tumorigenesis and metastasis pathways (Fig. 6H). Additionally, we identified 169 genes upregulated by Mir100hg overexpression and rescued by GNE, hypothesizing their regulation by the Mir100hg-H3K14la axis (Fig. 6I). Among these, 58% were associated with tumor metastasis (Fig. 6J), and 70% of these metastasis-associated genes showed significant H3K14la enrichment at the promoter region (Fig. 6K). Expression trends of several tumor metastasis-related genes increased in the OE-Mir100hg group and decreased following GNE addition (Fig. 6L). *PTGS2* was chosen for detailed analysis, showing significant increases in expression and H3K14la peaks in the OE-Mir100hg group, which decreased following GNE addition (Fig. 6M). Similarly, 145 genes regulated by the Mir100hg-H3K14la axis in the GNE and GNE+NALA groups. (Fig. S6A–E). These changes in the expression of tumor metastasis-associated genes and the H3K14la peaks in their promoters were highly correlated between the OE-Mir100hg group and the other groups (Fig. 6N). These findings suggest that Mir100hg enhances the metastatic potential of lung cancer cells by facilitating the transcription of tumor metastasis-related genes via H3K14la.

To ascertain the role of the Mir100hg-H3K14la axis in lung cancer metastasis, five key genes were identified through CUT&Tag, RNA-Seq, RT-PCR and prognosis analysis (Fig. 7A). Analysis of the TCGA-LUAD database confirmed the high expression of these five genes in lung adenocarcinoma compared to non-cancerous tissues (Fig. 7B). Compared to the control group, overexpression of Mir100hg significantly increased H3K14 modifications near the TSS and expression levels of these five genes. Under Mir100hg overexpression, GNE reduced the H3K14 modifications and expression levels of these genes, while NALA significantly restore them (Fig. 7C). Furthermore, survival analysis suggested that high

(See figure on next page.)

Fig. 5 Mir100hg facilitates lung cancer cell metastasis by enhancing lactylation. **A** Metabolomics heatmap; **B** Global lactylation and H3K14la levels detected by Western blot (WB); **C, D** Immunofluorescence detection of global lactylation and H3K14la levels; **E** Schematic diagram illustrating glycolytic steps affected by various drugs and inhibitors; **F** Global lactylation and H3K14la levels in OE-Mir100hg cells post-GNE treatment and subsequent NALA exposure; **G** Transwell of migration and invasion ability of LLC cells after si-Ldha and the counting bar chart. **H** Transwell migration and invasion assays of LLC cells post-GNE and NALA and the counting bar chart (* $p < 0.05$, ** $p < 0.01$, *** $p < 0.001$)

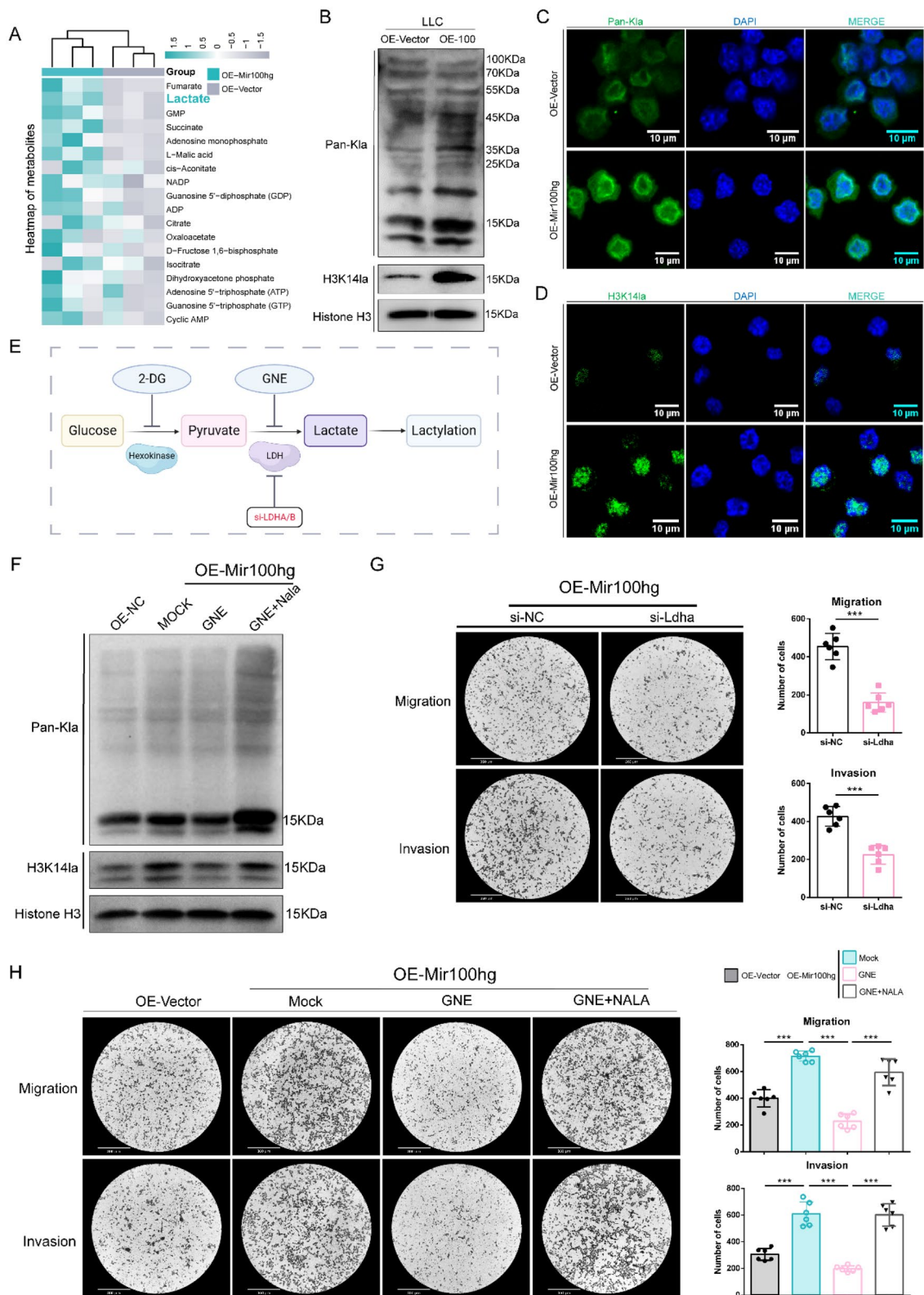


Fig. 5 (See legend on previous page.)

expression of these genes correlated with significantly lower overall survival in lung adenocarcinoma patients. Lastly, following siRNA-mediated knockdown of these five genes, transwell assays were performed. As shown in Fig. 7D, the knockdown of the five genes significantly inhibited lung cancer cell migration.

Collectively, our findings suggest that *Lman1*, *Ostc*, *P4ha1*, *Tex30*, and *Tmem65* are downstream genes promoting tumor metastasis, influenced by the Mir100hg-H3K14la regulatory axis in lung cancer.

Discussion

Cancer stem cells (CSCs) play crucial roles in tumor progression and metastasis, yet the mechanisms by which they influence the tumor microenvironment remain poorly understood. A critical gap in our knowledge has been how CSCs communicate with and modify the behavior of non-CSC tumor cells. Our study addresses this gap by revealing a novel mechanism through which CSCs enhance the metastatic potential of non-CSCs via exosomal transfer of the lncRNA Mir100hg. Our previous work identified that Mir100hg can regulate metastasis through miR-15a-5p/31-5p [20]. Here, we significantly extend these findings by uncovering a complex regulatory network involving nuclear-cytoplasmic trafficking, metabolic reprogramming, and epigenetic modification.

In this study, we have made the following new findings:

1. HNRNPs regulates the cytoplasmic translocation of nuclear Mir100hg and its entry into exosomes in CSCs.

The biological function and mechanism of action of a lncRNA depends on its intracellular localization [35]. Within the nucleus, lncRNAs are capable of interacting with a multitude of molecular entities exerting regulatory influences over chromosomal architecture and functionality. In the cytoplasmic domain, the roles of lncRNAs extend to the mediation of signal transduction pathways, translational machineries, and the post-transcriptional modulation of gene expression. The nuclear-cytoplasmic translo-

cation of lncRNAs is a complex biological process [36]. We uncovered a novel distinction in the nuclear and cytoplasmic localization of Mir100hg between lung CSCs and non-CSCs. Mechanistically, HNRNP F facilitates the translocation of Mir100hg from nucleus to cytoplasm and maintains its cytoplasmic presence in CSCs, which is crucial for its packaging into exosomes. However, our results indicate that while HNRNP F is involved in the nucleocytoplasmic translocation of Mir100hg, it is likely one of several factors in this process, as its knockdown did not completely inhibit Mir100hg's cytoplasmic localization.

Notably, inhibitors targeting the PI3K/AKT signaling pathway significantly reduce HNRNPF expression and impact tumor metastasis [37]. Given that the PI3K/AKT pathway is aberrantly activated in CSCs, these findings suggest a potential link between PI3K/AKT signaling, HNRNPF expression, and tumor metastasis. While our current study provides comprehensive evidence for the roles of HNRNPF and HNRNPA2B1 through multiple experimental approaches including RNA pulldown, RIP assays, and functional validation, future structural studies employing point mutations and competitive binding assays could further elucidate the precise molecular interfaces mediating these protein-RNA interactions. Future studies will also focus on investigating the regulation of HNRNPF by the PI3K/AKT pathway and how HNRNPA2B1 mediates the selective entry of Mir100hg into exosomes, which will provide insights into the fundamental mechanisms of exosomal lncRNA transport in the tumor microenvironment. Such detailed molecular characterization could potentially reveal targetable interfaces for therapeutic intervention in the exosomal transport of oncogenic lncRNAs.

2. Mir100hg regulates ALDOA expression by OTUD4-mediated de-ubiquitination and by targeting miR-15a-5p/31-5p

(See figure on next page.)

Fig. 6 Multi-omics analysis reveals the involvement of the Mir100hg-H3K14la axis in the transcription of tumor metastasis-related genes. **A** Bar graph showing the number of H3K14la peaks enriched across four groups; **B** Heatmap of H3K14la enrichment in TSS regions across four groups; **C** Enrichment of H3K14la in TSS regions of genes exhibiting varied expression levels in RNA-Seq; **D** Differential chromatin opening in H3K14la-enriched genes within TSS regions; **E** Differential heatmap in RNA-Seq of upregulated genes in OE-Mir100hg and corresponding TSS region heatmap in CUT&Tag; **F** GSEA analysis indicating enrichment of differentially expressed genes in OE-Mir100hg within tumor metastasis-related gene set; **G** Pie chart of the percentage of H3K14la-enriched genes among upregulated genes in OE-Mir100hg group; **H** KEGG analysis of pathways associated with H3K14LA-enriched upregulated genes; **I-L** Display of genes rescued post-addition of GNE in OE-Mir100hg group; **M** Ptg2 peaks identified in RNA-Seq and CUT&Tag; **N** Heatmap of TSS region enrichment for tumor metastasis-related genes in CUT&Tag and log fold change (logFC) heatmap in RNA-Seq (*p < 0.05, **p < 0.01, ***p < 0.001)

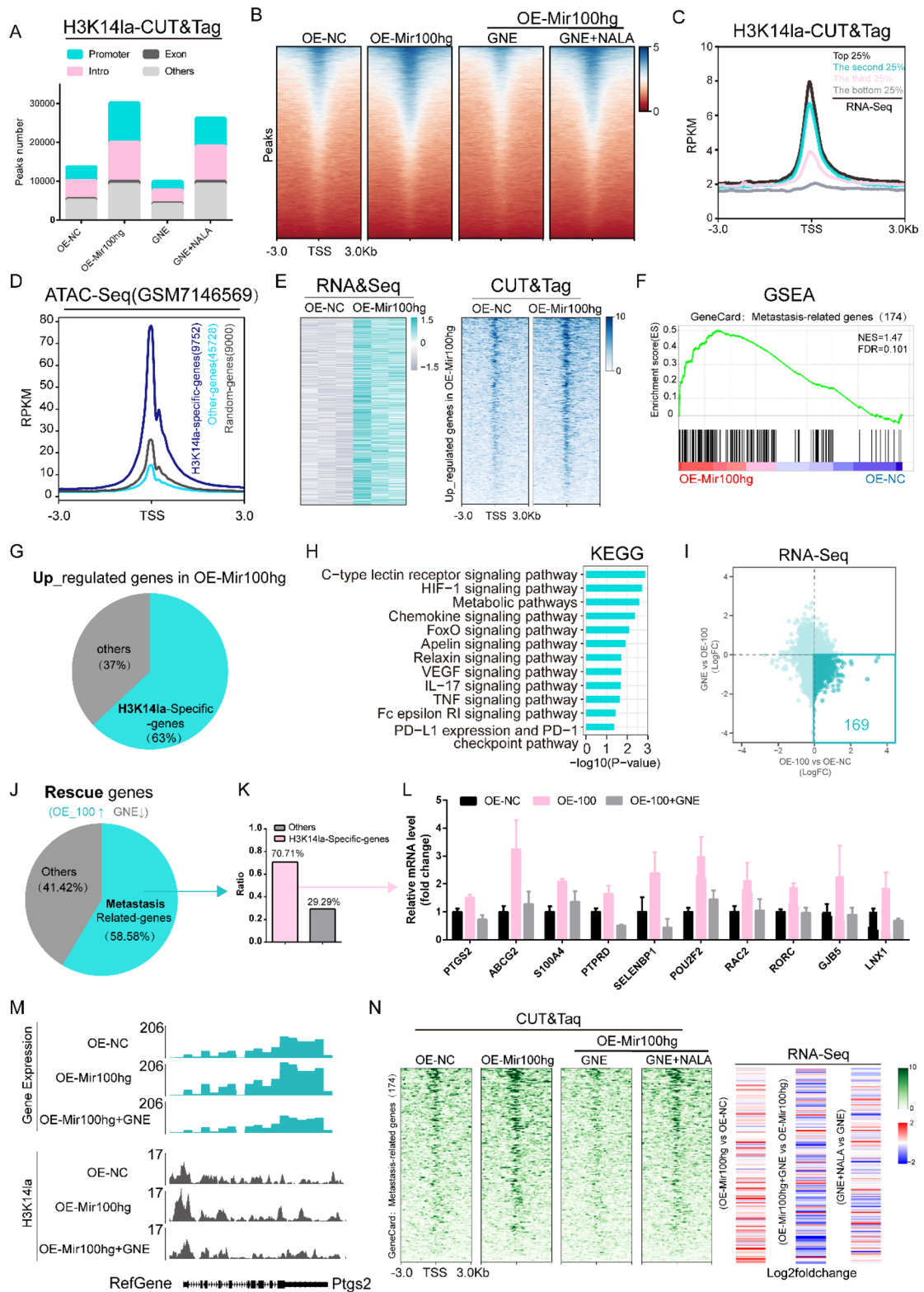


Fig. 6 (See legend on previous page.)

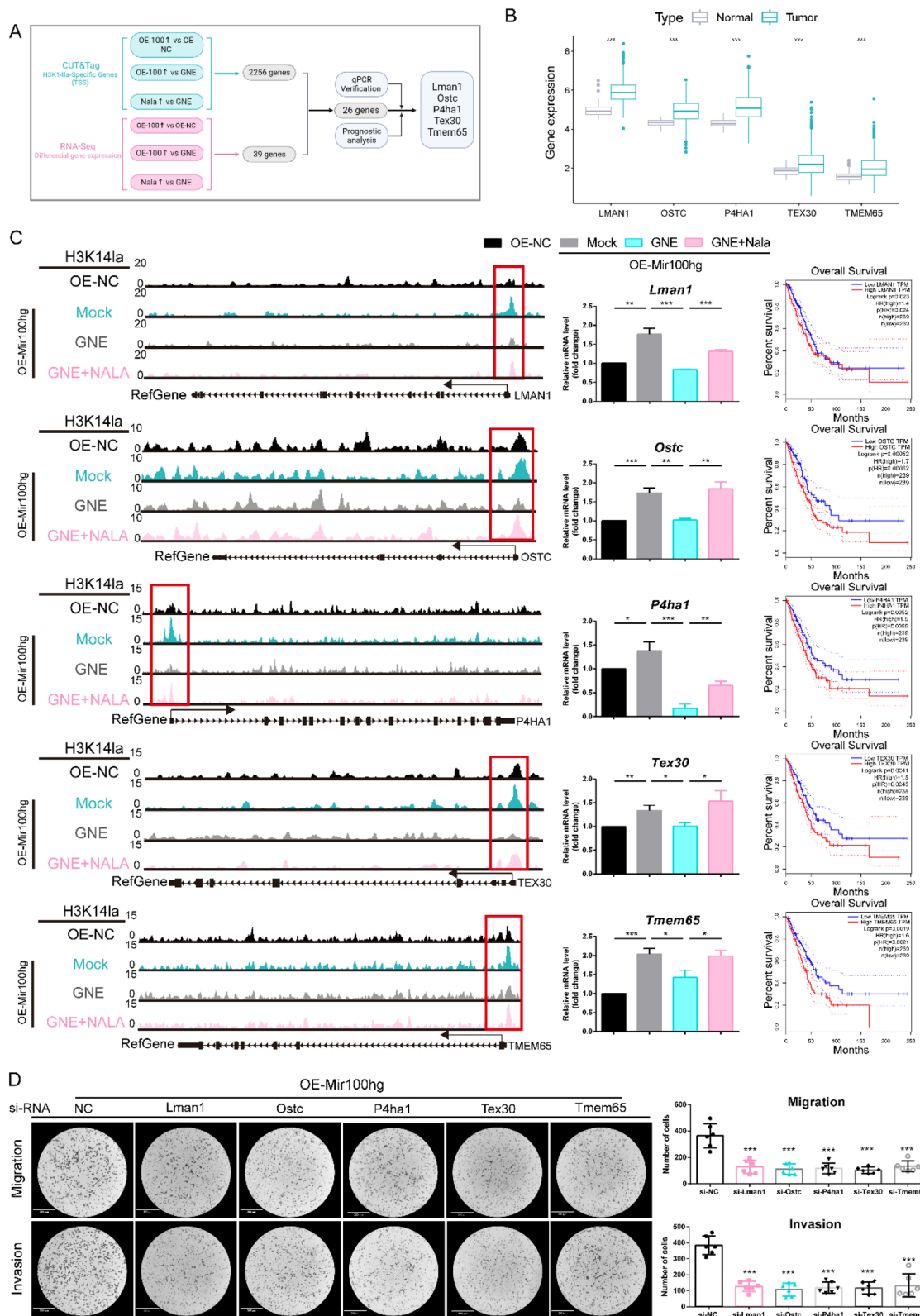


Fig. 7 The Mir100hg-H3K14 lactylation axis enhances the expression of genes associated with tumor metastasis. **A** Flow chart for gene screening process; **B** Boxplot of LMN1, OSTC, P4HA1, TEX30, and TMEM65 gene expression differences in TCGA-LUAD; **C** Lman1/Ostc/P4ha1/Tex30/Tmem65 in CUT&Tag peak figure display, mRNA expression changes and survival analysis; **D** Transwell for cell migration and invasion post-knockdown of LMAN1, OSTC, P4HA1, TEX30, and TMEM65 and the counting bar chart (* $p < 0.05$, ** $p < 0.01$, *** $p < 0.001$)

Our study revealed that Mir100hg regulates ALDOA expression through two distinct mechanisms. The first mechanism involves the competing endogenous RNA (ceRNA) network, a concept first proposed by Salmena et al. in 2011 [38]. The ceRNA hypothesis suggests that RNA transcripts can regulate each other's expression by competing for shared microRNAs, functioning as molecular sponges to sequester microRNAs and prevent them from binding to their target mRNAs [39]. This mechanism has been increasingly recognized as a crucial regulatory layer in cancer development and progression [40]. For instance, in hepatocellular carcinoma, the lncRNA HULC acts as a ceRNA to regulate PTEN expression by sequestering miR-485-5p [41]. Similarly, in breast cancer, the lncRNA NEAT1 functions as a ceRNA for miR-124, thereby regulating STAT3-mediated cancer progression [42]. In our study, Mir100hg functions as a ceRNA by competitively binding to miR-15a-5p and miR-31-5p, thereby preventing these microRNAs from suppressing ALDOA expression. This finding adds to the growing body of evidence supporting the importance of ceRNA networks in cancer progression.

The second mechanism involves post-translational modification, where Mir100hg acts as a molecular scaffold to facilitate the interaction between ALDOA and the deubiquitinating enzyme OTUD4, preventing ALDOA ubiquitination and increasing its protein abundance. This dual-regulatory mechanism is particularly noteworthy as it demonstrates that lncRNAs can simultaneously control gene expression at both transcriptional and post-translational levels. Our RNA pull-down assays further revealed that Mir100hg contains multiple protein-interacting domains, with distinct fragments (S1/S3 and S1/S2) mediating interactions with different protein partners. This structural versatility enables Mir100hg to function as an effective molecular scaffold, coordinating various regulatory processes. Future studies will focus on characterizing the specific binding sites and understanding how these multiple regulatory mechanisms are coordinated in cancer progression.

3. H3K14 lactylation represents a specific histone modification linking metabolic state to gene regulation. Among various histone lysine residues, we found H3K14 exhibits unique sensitivity to cellular lactate levels. Through metabolomic analysis and FilaNuc lactate sensor detection, we demonstrated that Mir100hg-induced ALDOA activation leads to increased nuclear lactate accumulation. Recent studies have revealed that lactylation is achieved through a two-step enzymatic cascade: first, lactate is con-

verted to lactyl-CoA by specific synthetases like GTPSCS and ACSS2 [43, 44]; then lactyltransferases such as p300/KAT2A transfer the lactyl group to specific lysine residues [44, 45]. Notably, we found that elevated lactate preferentially enhances H3K14 lactylation compared to other lysine residues (H3K9, H3K18, and H4K16), suggesting unique structural properties of H3K14 that facilitate its recognition by lactylation machinery.

The site-specificity of H3K14 lactylation is further validated by our pharmacological studies and mechanistic analyses. Treatment with glycolysis inhibitor 2-DG or LDHA inhibitor GNE140 significantly reduced H3K14 lactylation levels, while sodium lactate supplementation restored these effects. This dynamic response suggests the existence of dedicated enzymatic machinery for H3K14 lactylation. Recent structural studies have shown that specific lactyltransferases contain recognition motifs that preferentially target H3 histone lactylation, distinguishing it from other lysine residues [46]. The unique position of H3K14 in the histone tail and its surrounding amino acid sequence likely contribute to this preferential modification, providing a molecular basis for the observed site-specificity of lactylation. Future studies will aim to elucidate this process further, focusing on lactylation's impact on chromatin structure and gene expression. These studies will involve identifying and characterizing enzymes involved in lactylation and delactylation, determining enzyme activation/inhibition mechanisms, and examining lactylation's role in cellular metabolism and signaling pathways.

Conclusions

In summary, our study elucidates the regulatory mechanism underlying the complex process of lncRNA transfer between heterogeneous tumor cells via exosomes, aided by multiple binding proteins. This transfer influences lactylation in recipient cells and enhances the metastatic potential of tumor cell populations. Our findings unveil the intricate and extensive regulatory network within tumor cell populations, offering new insights into tumor metastasis.

Supplementary Information

The online version contains supplementary material available at <https://doi.org/10.1186/s12951-025-03198-0>.

- Supplementary Material 1.
- Supplementary Material 2.
- Supplementary Material 3.
- Supplementary Material 4.

Acknowledgements

Not applicable.

Author contributions

Lei Shi, Bowen Li, Jiyu Tan and Ling Zhu conducted the experiments and analyzed the data. Lei Shi was responsible for writing the manuscript. Sicheng Zhang, Yuhang Zhang, Meng Xiang, Jie Li, Yan Chen, Xue Han, Jiacheng Xie, Yao Tang participated in the conduction of this study. Jianyu Wang, Jingyu Li and H. Rosie Xing designed and oversaw the execution of this study and contributed to the writing of this manuscript.

Funding

This work was supported by the National Natural Science Fund (Grant No. 82073277 and 82173247), the Science and Technology Project Affiliated to the Education Department of Chongqing (Grant No. KJQN202100404), Science and Technology Project of Chongqing Yuzhong District (Grant No. 20200110), Postgraduate Research Innovation Project of Chongqing (CYS23363) and Project of Chongqing Natural Science Foundation Innovation and Development Fund (Municipal Education Commission) (Grant No. 2022NSCQ-LZX0020).

Availability of data and materials

The datasets used and analysed during the current study are available from the corresponding author on reasonable request.

Declarations**Ethics approval and consent to participate**

Not applicable.

Consent for publication

Not applicable.

Competing interests

The authors declare no competing interests.

Author details

¹State Key Laboratory of Ultrasound in Medicine and Engineering, College of Biomedical Engineering, Chongqing Medical University, Chongqing 400016, China. ²Molecular Biology Laboratory of Respiratory Disease, Key Laboratory of Clinical Laboratory Diagnostics (Ministry of Education), College of Laboratory Medicine, Chongqing Medical University, Chongqing 400016, China. ³Chongqing Key Laboratory of Human Embryo Engineering and Precision Medicine, Center for Reproductive Medicine, Chongqing Health Center for Women and Children, Women and Children's Hospital of Chongqing Medical University, Chongqing 400016, China. ⁴Department of Medical Oncology, Clinical Oncology School of Fujian Medical University, Fujian Cancer Hospital, Fuzhou 350000, Fujian Province, China.

Received: 3 January 2025 Accepted: 2 February 2025

Published online: 28 February 2025

References

- Li C, Lei S, Ding L, et al. Global burden and trends of lung cancer incidence and mortality. *Chin Med J (Engl)*. 2023;136(13):1583–90.
- Xie S, Wu Z, Qi Y, Wu B, Zhu X. The metastasizing mechanisms of lung cancer: recent advances and therapeutic challenges. *Biomed Pharmacother*. 2021;138: 111450.
- Fares J, Fares MY, Khachfe HH, Salhab HA, Fares Y. Molecular principles of metastasis: a hallmark of cancer revisited. *Signal Transduct Target Ther*. 2020;5:28.
- Rowbotham SP, Goruganthu M, Arasada RR, et al. Lung cancer stem cells and their clinical implications. *Cold Spring Harb Perspect Med*. 2022;12(4): a041270.
- Nassar D, Blanpain C. Cancer stem cells: basic concepts and therapeutic implications. *Annu Rev Pathol*. 2016;11:47–76.
- Kalluri R, LeBleu VS. The biology, function, and biomedical applications of exosomes. *Science*. 2020;367:6478.
- Kok VC, Yu CC. Cancer-derived exosomes: their role in cancer biology and biomarker development. *Int J Nanomed*. 2020;15:8019–36.
- Liu J, Ren L, Li S, et al. The biology, function, and applications of exosomes in cancer. *Acta Pharm Sin B*. 2021;11(9):2783–97.
- Xu Z, Chen Y, Ma L, et al. Role of exosomal non-coding RNAs from tumor cells and tumor-associated macrophages in the tumor microenvironment. *Mol Ther*. 2022;30(10):3133–54.
- Liu SJ, Dang HX, Lim DA, Feng FY, Maher CA. Long noncoding RNAs in cancer metastasis. *Nat Rev Cancer*. 2021;21(7):446–60.
- Malla RR, Padmaraju V, Marni R, Kamal MA. Natural products: potential targets of TME related long non-coding RNAs in lung cancer. *Phytomedicine*. 2021;93: 153782.
- Zhou L, Zhu Y, Sun D, Zhang Q. Emerging roles of long non-coding RNAs in the tumor microenvironment. *Int J Biol Sci*. 2020;16(12):2094–103.
- Behera J, Kumar A, Voor MJ, Tyagi N. Exosomal lncRNA-H19 promotes osteogenesis and angiogenesis through mediating Angpt1/Tie2-NO signaling in CBS-heterozygous mice. *Theranostics*. 2021;11(16):7715–34.
- Ren J, Ding L, Zhang D, et al. Carcinoma-associated fibroblasts promote the stemness and chemoresistance of colorectal cancer by transferring exosomal lncRNA H19. *Theranostics*. 2018;8(14):3932–48.
- Zhang D, Tang Z, Huang H, et al. Metabolic regulation of gene expression by histone lactylation. *Nature*. 2019;574(7779):575–80.
- Lv X, Lv Y, Dai X. Lactate, histone lactylation and cancer hallmarks. *Expert Rev Mol Med*. 2023;25: e7.
- Jiang J, Huang D, Jiang Y, et al. Lactate modulates cellular metabolism through histone lactylation-mediated gene expression in non-small cell lung cancer. *Front Oncol*. 2021;11: 647559.
- Wang J, Liu Z, Xu Y, et al. Enterobacterial LPS-inducible LINC00152 is regulated by histone lactylation and promotes cancer cells invasion and migration. *Front Cell Infect Microbiol*. 2022;12: 913815.
- Wang J, Sun Z, Liu Y, et al. Comparison of tumor biology of two distinct cell sub-populations in lung cancer stem cells. *Oncotarget*. 2017;8(57):96852–64.
- Shi L, Li B, Zhang Y, et al. Exosomal lncRNA Mir100hg derived from cancer stem cells enhance glycolysis and promote metastasis of lung adenocarcinoma through microRNA-15a-5p/31-5p. *Cell Commun Signal*. 2023;21(1):1–248.
- Wang S, Ke H, Zhang H, et al. lncRNA MIR100HG promotes cell proliferation in triple-negative breast cancer through triplex formation with p27 loci. *Cell Death Dis*. 2018;9(8):805.
- Su X, Teng J, Jin G, et al. ELK1-induced upregulation of long non-coding RNA MIR100HG predicts poor prognosis and promotes the progression of osteosarcoma by epigenetically silencing LATS1 and LATS2. *Biomed Pharmacother*. 2019;109:788–97.
- Emmrich S, Streltsov A, Schmidt F, et al. lincRNAs MONC and MIR100HG act as oncogenes in acute megakaryoblastic leukemia. *Mol Cancer*. 2014;13:171.
- Faubert B, Solmonson A, DeBerardinis RJ. Metabolic reprogramming and cancer progression. *Science*. 2020;368:6487.
- Zhang H, Xu R, Li B, et al. lncRNA NEAT1 controls the lineage fates of BMSCs during skeletal aging by impairing mitochondrial function and pluripotency maintenance. *Cell Death Differ*. 2022;29(2):351–65.
- Park MK, Zhang L, Min KW, et al. NEAT1 is essential for metabolic changes that promote breast cancer growth and metastasis. *Cell Metab*. 2021;33(12):2380–2397.e9.
- Rinn JL, Chang HY. Genome regulation by long noncoding RNAs. *Annu Rev Biochem*. 2012;81:145–66.
- Wang KC, Chang HY. Molecular mechanisms of long noncoding RNAs. *Mol Cell*. 2011;43(6):904–14.
- Mevissen TE, Hospenthal MK, Geurink PP, et al. OTU deubiquitinases reveal mechanisms of linkage specificity and enable ubiquitin chain restriction analysis. *Cell*. 2013;154(1):169–84.
- Oikawa D, Shimizu K, Tokunaga F. Pleiotropic roles of a KEAP1-associated deubiquitinase, OTUD1. *Antioxidants (Basel)*. 2023;12(2):350.
- Wilde ML, Ruparel U, Klemm T, et al. Characterisation of the OTU domain deubiquitinase complement of *Toxoplasma gondii*. *Life Sci Alliance*. 2023;6(6): e202201710.
- Chu Y, Kang Y, Yan C, et al. LUBAC and OTULIN regulate autophagy initiation and maturation by mediating the linear ubiquitination and the stabilization of ATG13. *Autophagy*. 2021;17(7):1684–99.

33. Schubert AF, Nguyen JV, Franklin TG, et al. Identification and characterization of diverse OTU deubiquitinases in bacteria. *EMBO J.* 2020;39(15): e105127.
34. Li X, Zhang Y, Xu L, et al. Ultrasensitive sensors reveal the spatiotemporal landscape of lactate metabolism in physiology and disease. *Cell Metab.* 2023;35(1):200-211.e9.
35. Bridges MC, Daulagala AC, Kourtidis A. LNCcation: lncRNA localization and function. *J Cell Biol.* 2021;220(2): e202009045.
36. Ashkenazy-Titelman A, Atrash MK, Boocholez A, Kinor N, Shav-Tal Y. RNA export through the nuclear pore complex is directional. *Nat Commun.* 2022;13(1):5881.
37. Li F, Xie W, Fang Y, et al. HnRNP-F promotes the proliferation of bladder cancer cells mediated by PI3K/AKT/FOXO1. *J Cancer.* 2021;12(1):281–91.
38. Salmena L, Poliseno L, Tay Y, Kats L, Pandolfi PP. A ceRNA hypothesis: the Rosetta Stone of a hidden RNA language? *Cell.* 2011;146(3):353–8.
39. Quinn JJ, Chang HY. Unique features of long non-coding RNA biogenesis and function. *Nat Rev Genet.* 2016;17(1):47–62.
40. Tay Y, Rinn J, Pandolfi PP. The multilayered complexity of ceRNA crosstalk and competition. *Nature.* 2014;505(7483):344–52.
41. Wang Y, Lu JH, Wu QN, et al. lncRNA LINRIS stabilizes IGF2BP2 and promotes the aerobic glycolysis in colorectal cancer. *Mol Cancer.* 2019;18(1):174.
42. Pang Y, Wu J, Li X, et al. NEAT1/miR-124/STAT3 feedback loop promotes breast cancer progression. *Int J Oncol.* 2019;55(3):745–54.
43. Liu R, Ren X, Park YE, et al. Nuclear GTPSCS functions as a lactyl-CoA synthetase to promote histone lactylation and gliomagenesis. *Cell Metab.* 2024. <https://doi.org/10.1016/j.cmet.2024.11.005>.
44. Zhu R, Ye X, Lu X, et al. ACSS2 acts as a lactyl-CoA synthetase and couples KAT2A to function as a lactyltransferase for histone lactylation and tumor immune evasion. *Cell Metab.* 2024. <https://doi.org/10.1016/j.cmet.2024.10.015>.
45. Minami E, Sasa K, Yamada A, et al. Lactate-induced histone lactylation by p300 promotes osteoblast differentiation. *PLoS ONE.* 2023;18(12): e0293676.
46. Huang Y, Wang C, Zhou T, et al. Lumican promotes calcific aortic valve disease through H3 histone lactylation. *Eur Heart J.* 2024;45(37):3871–85.

Publisher's Note

Springer Nature remains neutral with regard to jurisdictional claims in published maps and institutional affiliations.